Tertiary and quaternary structure remodeling by occupancy of the substrate binding pocket in a large glutamate dehydrogenase

Melisa Lázaro [1,#], Nicolás Chamorro [2,#], Jorge P. López-Alonso [3,4], Diego Charro [1], Rodolfo M. Rasia [2,5], Gonzalo Jiménez-Osés [1,6], Mikel Valle [1,*], María-Natalia Lisa [2,4,*]

[1] Center for Cooperative Research in Biosciences (CIC bioGUNE), Basque Research and Technology Alliance (BRTA), Bizkaia Technology Park, Building 801A, 48160 Derio, Spain.

[2] Instituto de Biología Molecular y Celular de Rosario (IBR CONICET-UNR), Ocampo y Esmeralda, Rosario S2002LRK, Argentina.

[3] Instituto Biofisika (UPV/EHU, CSIC), 48940 Leioa, Spain.

[4] Basque Resource for Electron Microscopy, 48940 Leioa, Spain.

[5] Plataforma de Biología Estructural y Metabolómica (PLABEM), Ocampo y Esmeralda, Rosario S2002LRK, Argentina.

[6] Ikerbasque, Basque Foundation for Science, 48013 Bilbao, Spain.

# Equal contribution

* Correspondence: MNL: lisa@ibr-conicet.gov.ar; MV: mvalle@cicbiogune.es

ABSTRACT

Glutamate dehydrogenases (GDHs) catalyze the oxidative deamination of L-glutamate to 2-oxoglutarate using $NAD(P)^+$ as a cofactor. The large type of GDHs (L-GDHs) displays a dynamic homotetrameric architecture that alternates between open and closed states. The catalytic mechanism and the role of the large conformational changes of L-GDHs in enzymatic function are unknown. Here, we explore by cryoEM the structure and the conformational space of the mycobacterial L-GDH composed of 180 kDa subunits (mL-GDH_{180}) when incubated with L-glutamate and NAD^+. Classification of the heterogeneous population of tetramers into different subsets reveals opening-closing motions and sorting of individual subunits resolves the occupancy of the cofactor and substrate binding pockets. Maps show that ligand binding to the glutamate binding pocket is accompanied by structural changes in a distant region that mediates a novel interaction between the catalytic domains of neighboring subunits in closed tetrameric states. Our findings indicate that the occupancy of the orthosteric site of mL-GDH_{180} is linked to a remodeling of the enzyme tertiary and quaternary structure.

INTRODUCTION

Amino acid dehydrogenases have been a focus of interest for decades due to their physiological roles and potential industrial applications. Among them, glutamate dehydrogenases (GDHs; EC 1.4.1.2) catalyze the reaction L-glutamate + $NAD(P)^+$ + H_2O <=> 2-oxoglutarate + NAD(P)H + H^+ + NH_3, at the crossroads of carbon and nitrogen metabolism. These enzymes are oligomeric and are classified based on the molecular weight of their subunits. Small GDHs (S-GDHs), present in prokaryotes and eukaryotes, are composed of 50 kDa subunits [1]. The conserved catalytic domain spans nearly the entire length of the primary structure of S-GDHs and provides the oligomerization surfaces. Biochemical and structural studies of diverse S-GDHs have allowed elucidating their catalytic and regulatory mechanisms. However, knowledge about such aspects for large GDHs (L-GDHs) present in prokaryotes and lower eukaryotes is comparatively scarce [2]. Among these enzymes are L-GDHs composed of 115 kDa subunits ($L\text{-}GDHs_{115}$) and those with 180 kDa subunits ($L\text{-}GDHs_{180}$), such as the $L\text{-}GDH_{180}$ found in mycobacteria ($mL\text{-}GDH_{180}$). Distinctive long N- and C-terminal regions flank the catalytic domain of L-GDHs [3].

In a previous work we discovered that the $L\text{-}GDH_{180}$ from *Mycobacterium smegmatis* ($mL\text{-}GDH_{180}$; 76% sequence identity with the $L\text{-}GDH_{180}$ from *Mycobacterium tuberculosis*) assembles into a homo-tetramer, adopting a quaternary structure that is radically different from that of S-GDHs [3]. Such architecture depends on interactions provided by an N-terminal region containing ACT- and PAS-type domains [4,5] with regulatory potential as well as a C-terminal domain of unknown function, both flanking the catalytic domain in $mL\text{-}GDH_{180}$ subunits.

Here we report cryoEM evidence of up to 3 Å resolution of alternative conformers of $mL\text{-}GDH_{180}$ detected in the presence of NAD^+ and L-glutamate. We found that ligand binding to the glutamate binding pocket is accompanied by changes in the tertiary structure in a

region distant from the active site, which in turn promotes interactions between the catalytic domains of neighboring monomers and modifications of the quaternary structure. Despite decades of research into the molecular basis of GDHs activity and regulation, experimental structural information on enzyme-cofactor-L-glutamate ternary complexes is still scarce, especially for NAD^+-dependent enzymes. Here, we present cryoEM evidence for enzyme species present upon incubation with L-glutamate and NAD^+ of a key L-GDH_{180} for the virulence of a long-attacked pathogen [6].

METHODS

Protein production

Plasmid pLIC-His-mL-GDH_{180} [3] was used to produce N-terminally His6-tagged mL-GDH180 (MSMEG_4699, Uniprot A0R1C2) in *E. coli* cells. Transformed *E. coli* BL21(DE3) cells were grown at 37 °C in LB broth supplemented with 100 µg/ml ampicillin until reaching 0.8 units of optical density at 600 nm. Protein expression was then induced by adding isopropyl β-D-1-thiogalactopyranoside (IPTG) to a final concentration of 0.5 mM and incubation was continued for 18 hours at 14 °C. The culture was centrifuged and the pellet was resuspended in 25 mM Hepes, 500 mM NaCl, 10 % V/V glycerol, 10 mM imidazole, pH 8.0. The suspension was supplemented with 0.01 µg/mL DNAse, 4 µM $MgSO_4$ and the protease inhibitor cOmplete™ EDTA-free Protease Inhibitor Cocktail (Roche). Cells were then sonicated and the mixture was clarified by centrifugation. The supernatant was loaded onto a HisTrap HP column (Cytiva) equilibrated with buffer 25 mM Hepes, 500 mM NaCl, 10% v/v glycerol, 20 mM imidazole, pH 8.0, and His6-tagged mL-GDH_{180} was purified by applying a linear imidazole gradient (20-500 mM). The protein was then further purified by size-exclusion chromatography, using a Superose 6 10/300 GL column (Cytiva) equilibrated in 20 mM Mes, 300 mM NaCl, pH 6.5. mL-GDH_{180} containing fractions, as confirmed by SDS-PAGE, were pooled and used immediately or stored at -80 °C for use in subsequent studies. The protein was quantified by electronic absorption using the molar absorption coefficient of 171,090 M^{-1} cm^{-1}, predicted from the amino acid sequence by the ProtParam tool (http://web.expasy.org/protparam/).

Steady state kinetics

Reactions were performed at 25 °C, using 11.2 nM mL-GDH_{180}. Oxidative deamination of L-glutamate catalyzed by mL-GDH_{180} was monitored by following the increase in absorbance at 340 nm resulting from NADH production. To calculate reaction rates, the

97 molar extinction coefficient 6220 M^{-1} cm^{-1} for NADH at 340 nm was used. The kinetic
98 parameters k_{cat} and K_M were derived by fitting the Michaelis-Menten equation to initial
99 rates measured in 100 mM NaH_2PO_4/Na_2HPO_4, pH 7.0, recorded on a Shimadzu UV-120-
100 02 spectrophotometer. k_{cat} and K_M values and their errors reported correspond to the
101 mean and maximum dispersion observed, respectively, between at least two independent
102 measurements performed with different protein preparations. The catalytic efficiency
103 (k_{cat}/K_M) was calculated as the quotient between k_{cat} and K_M, and its error was obtained by
104 propagating the error of such parameters.
105
106 **Cryo-electron microscopy**
107 4 µl of a mixture containing 42 mM L-glutamate, 4 mM NAD^+ and 0.125 mg/ml mL-GDH_{180}
108 was prepared in 20 mM Mes, 300 mM NaCl, pH 6.5, at 10 ºC, while monitoring NADH
109 production. Samples were applied to Quantifoil R2/2 holey carbon grids and vitrified using
110 a Leica EM GP2 within the first minute after mixing, ensuring the presence of catalytically
111 active enzyme molecules. In addition, a similar protein solution was applied onto the same
112 type of grids bearing an additional thin layer of carbon. Vitrification on these two types of
113 grids was required to obtain top and side views of mL-GDH_{180} tetramers. Data collection
114 was carried out in a ThermoFisher Titan Krios G4 transmission electron microscope paired
115 with a Gatan BioContinuum Imaging Filter and a K3 direct electron detector device, at the
116 BREM (Basque Resource for Electron Microscopy). 23,747 and 19,038 movie frames were
117 acquired for the sample on Q2/2 grids and grids supplemented with an additional thin layer
118 of carbon, respectively. Both collections were performed at a nominal magnification of
119 ×130,000, resulting in a sampling of 0.6462 Å/pixel. Each movie contained 50 frames with
120 an accumulated dose of 49 $e^-/Å^2$. Movie frames were aligned using MotionCor2 [7] and the
121 final average included all dose-weighted frames.

The contrast transfer function (CTF) of the micrographs was estimated using CTFFIND4 [8]. Particles were automatically selected from the micrographs using autopicking from RELION-4 [9]. An initial set of 667,866 particles was subjected to 2D and 3D classification procedures. The 3D-classification with imposed D2 symmetry resulted in eight different classes, but only three achieved good definition and high resolution. Three different conformations were obtained, called the Open (37,641 particles), Closed1 (45,998 particles) and Closed2 (32,441 particles) conformations, with estimated resolutions of 3.88 Å, 3.54 Å and 3.57 Å, respectively. Each class was symmetry-expanded, the star files were joined (116,080x4, *i.e.* 464,320 particles) and an average 3D map of a subunit was refined using a mask and polished to a final resolution of 2.63 Å. A 3D classification within a sphere mask focused on the active site separated three different states: empty-monomer, with 131,216 particles and 3.07 Å of resolution, cofactor-monomer, with 168,668 particles and 2.95 Å of resolution, and cofactor/ligand-monomer, with 112,701 particles and 3.12 Å of resolution. These three groups were crossed with the three sets of particles obtained in the initial classification from the conformational changes of the tetramer, resulting into nine groups of particles that were refined independently. The three maps with signal in the cofactor and substrate binding pockets were subjected to polishing and ctfrefine to improve the resolution, each one coming from a conformation of the tetramer: Open-cofactor/ligand-monomer (3.23 Å), Closed1-cofactor/ligand-monomer (3.11 Å) and Closed2-cofactor/ligand-monomer (3.18 Å). The cryoEM density maps were postprocessed by local sharpening using EMReady [10], which improved the structural details and facilitated the atomic model building.

Model fitting into cryo-EM maps was performed using the programs UCSF Chimera [11], Coot [12] and phenix.real_space_refine [13]. From the 2.63 Å resolution cryoEM map of a mL-GDH_{180} monomer and an initial model of the protein built by AlphaFold 3 [14], a model of the polypeptide chain was refined which was then fitted into the other cryo-EM maps. After

removing parts of the model not defined in the maps, performing manual model building when necessary and placing ligands manually, using Coot [12], where appropriate, atomic coordinates and B-factors were refined using phenix.real_space_refine [13] with NCS and secondary structure restraints.

Figures were generated and rendered with UCSF Chimera [11] or PyMOL version 1.8.x (Schrödinger, LLC).

Cryo-EM maps obtained for mL-GDH_{180} were deposited in the Electron Microscopy Data Bank under the accession codes EMD-52419 (Open), EMD-52420 (Closed1), EMD-52421 (Closed2), EMD-52422 (empty-monomer), EMD-52423 (cofactor-monomer), EMD-52424 (cofactor/ligand-monomer), EMD-52425 (Open-cofactor/ligand-monomer), EMD-52426 (Closed1-cofactor/ligand-monomer), EMD-52427 (Closed2-cofactor/ligand-monomer), EMD-52428 (total-monomer) and EMD-52429 (Closed2-cofactor/ligand-tetramer). Atomic coordinates were deposited in the Protein Data Bank under the accession codes 9HUX (Open), 9HUY (Closed1), 9HUZ (Closed2), 9HV0 (empty-monomer), 9HV4 (cofactor-monomer), 9HV5 (cofactor/ligand-monomer) and 9HV6 (total-monomer).

164 **RESULTS**

165 **Three conformers of mL-GDH$_{180}$ detected upon incubation with L-glutamate and**
166 **NAD$^+$ reveal modulations of the enzyme quaternary structure**

167 To investigate the molecular basis of mL-GDH$_{180}$ activity, we first determined the kinetic
168 parameters for the oxidative deamination of L-glutamate catalyzed by the enzyme. The
169 estimated k_{cat}, K_M and k_{cat}/K_M values under steady state conditions, in 100 mM
170 NaH_2PO_4/Na_2HPO_4 at pH 7.0, were (20 ± 5) s^{-1}, (34 ± 7) mM and (0.6 ± 0.3) s^{-1} mM^{-1} for L-
171 glutamate, and (21 ± 5) s^{-1}, (0.26 ± 0.07) mM and (80 ± 40) s^{-1} mM^{-1} for NAD$^+$, respectively
172 (Figure S1). Then, single-particle cryoEM experiments were performed with mL-GDH$_{180}$ in
173 the presence of NAD$^+$ and L-glutamate, during the course of NADH production (see
174 Methods). As previously reported [3], 2D averages for side views of mL-GDH$_{180}$ tetramers
175 revealed a high degree of flexibility at distal ends, where ACT*1-2 and PAS domains
176 reside, and their corresponding densities vanish in cryoEM maps. A 3D-classification of
177 mL-GDH$_{180}$ particles was performed to distinguish alternate conformers of the enzyme.
178 Three mL-GDH$_{180}$ conformers were found, called the Open, Closed1 and Closed2
179 conformations (Figure 1, Table 1, Figure S2), for which the ACT*3 module, the helical
180 motif 3 (HM3), the catalytic domain and the C-terminal region were defined in each
181 monomer, achieving estimated resolutions of 3.88 Å, 3.54 Å and 3.57 Å, respectively. The
182 three conformers differ in the relative positions of the subunits (Figure 1A, Figure S3A and
183 Movie S1). The catalytic domains in mL-GDH$_{180}$ monomers in contact through their N-
184 terminal segments are closer to each other in the Closed conformations compared to the
185 Open form (Figure 1B).

186 A comparison of the atomic models derived from the obtained 3D cryoEM maps shed
187 initial insights on the molecular determinants involved in the modulation of the architecture
188 of mL-GDH$_{180}$. An average RMSD of 0.4 Å (1075 aligned residues) was estimated after
189 pairwise comparisons of monomers in the three mL-GDH$_{180}$ conformers, suggesting that

190 the observed conformational changes were largely related to modifications of the
191 quaternary structure. Consistent with this, the contact area at the AB-CD interface (Figure
192 S3B) is 550 Å^2, 750 Å^2 and 800 Å^2, while at the AD-BC interface it is 1200 Å^2, 1000 Å^2 and
193 1200 Å^2, as measured for the Open, Closed1 and Closed2 forms of mL-GDH$_{180}$,
194 respectively. At the AB-CD interface of mL-GDH$_{180}$ conformers, intersubunit contacts are
195 established by hydrogen bonds between residues of the ACT*3 domains in neighboring
196 monomers (Figure S3B and Table S1). Remarkably, a previously undetected interfacial
197 interaction was found between the side chains of Ser650 in the HM3 and Glu790 in the
198 catalytic domain, exclusively in the Closed2 mL-GDH$_{180}$ tetramer (Figure 1B and Figure
199 S3B). On the other hand, at the AD-BC interface, mL-GDH$_{180}$ monomers connect via
200 Asp1516:Arg1582 or Arg1504:Glu1562 salt bridges in the Open and Closed1 forms,
201 respectively, while both interactions were observed in the Closed2 conformer (Figure S3B
202 and Table S1). Additionally, in all three conformations extensive series of hydrogen bonds
203 are established that alternately link a conserved set of secondary structure elements in the
204 C-terminal domain. Most of the interfacial amino acids in mL-GDH$_{180}$ tetramers found upon
205 incubation with of NAD$^+$ and L-glutamate were previously identified as determinants of the
206 oligomeric state of the enzyme [3] and are conserved in diverse L-GDHs (Figure S4),
207 pointing out their functional relevance.
208 As HM3 in one monomer and the region including residue Glu790 in the catalytic domain
209 of another subunit approach, so do other portions of the catalytic domains in mL-GDH$_{180}$
210 monomers linked by the N-terminal segment (Figure 1B). Intriguingly, the density of the
211 zone 825-838 was poorly defined in the maps of the Open, Closed1 and Closed2 mL-
212 GDH$_{180}$ tetramers distinguished upon incubation with NAD$^+$ and L-glutamate. At the same
213 time, the nicotinamide portion of the cofactor molecule placed within the active site
214 displayed high mobility in the three enzyme conformers, although it appeared to decrease
215 in the Closed1 and Closed2 forms. When analyzing the active sites in mL-GDH$_{180}$

216 tetramers, no evidence was found for the presence of a chemical entity other than the
217 cofactor.
218
219 **Three conformers of mL-GDH$_{180}$ subunits reveal modulations in tertiary structure**
220 **associated with differential active site occupancies**
221 In order to clarify the lack of signal for a ligand other than the cofactor in the cryoEM maps
222 for mL-GDH$_{180}$ tetramers, we performed a hierarchical classification of all mL-GDH$_{180}$
223 subunits, whether they were part of the Open, Closed1 or Closed2 conformers, applying a
224 mask that covered the catalytic domain (Figure S2). In this classification we found three
225 forms for mL-GDH$_{180}$ monomers, called empty-monomer, cofactor-monomer and
226 cofactor/ligand-monomer, achieving estimated resolutions of 3.07 Å, 2.95 Å and 3.12 Å,
227 respectively (Figure 2 and Table 1). The empty-monomer map shows some density
228 beyond that attributable to the polypeptide chain in the cofactor binding pocket, but does
229 not indicate, however, strong binding to that site nor does it reveal any signal in the
230 substrate binding pocket. The cofactor-monomer map, on the other hand, clearly reveals a
231 cofactor molecule bound to the catalytic cavity of mL-GDH$_{180}$ and the cofactor/ligand-
232 monomer map discloses both the cofactor as well as an additional compound within the
233 active site of the enzyme. An average of all these variants resulted in a 2.63 Å resolution
234 map of a mL-GDH$_{180}$ monomer (Figure S5), which was used to unambiguously model the
235 polypeptide chain prior to subsequent refinement of atomic coordinates linked to species
236 with differential occupancy in the active site.
237 The atomic model derived from the empty-monomer map exposed the arrangement of
238 residues that, according to previous analyses [2,3], constitute the dinucleotide binding region
239 (DNBR) and the glutamate binding region (GluBR) of mL-GDH$_{180}$ (Figure 2). The cryoEM
240 maps of the cofactor- and cofactor/ligand- monomers of mL-GDH$_{180}$ allowed to
241 unambiguously position a NAD^+ molecule in extended conformation in the DNBR of mL-

242 GDH_{180} (Figure 2), with the pyrophosphate moiety located in the crevice formed between
243 strands β1 and β5 (residues 953-958 and 1070-1073, respectively) of the catalytic domain
244 subdomain II (SDII) and stabilized by a favorable interaction with the dipole of the helix
245 (residues 964-969) connecting strands β1 and β2 (residues 976-982), also called the
246 dinucleotide binding helix (Figure 3). Also, it was possible to unequivocally place the
247 adenine ring of NAD^+, to assign the conformation of the glycosidic bond to the
248 nicotinamide ring as *syn*, and to assign the conformation of the adenosine and
249 nicotinamide riboses to C2' *endo*, in agreement with previous reports for S-GDHs [15].
250 Differences were observed in the pattern of NAD^+-protein interactions established in
251 cofactor- and cofactor/ligand- mL-GDH_{180} subunits (Figure 2). In the cofactor-monomer,
252 the adenine ring of the dinucleotide interacts with the side chain (sc) of residue Tyr1079,
253 the 2' and 3' hydroxyl groups of the adenosine ribose point towards the surface of the
254 enzyme and hydrogen bond Asp983 (sc) and the main chain (mc) of Asp960, respectively,
255 phosphates interact with the amide nitrogen of Asp964 and Val965, the nicotinamide
256 ribose hydrogen bonds Gly1075 (mc) and Asn1115 (mc and sc), and the nicotinamide
257 amide contacts His923 (sc), Thr929 (sc) and Asp964 (sc). In the cofactor/ligand-monomer,
258 instead, the adenine of NAD^+ interacts with Tyr1079 (sc) as well as His984 (sc), both
259 hydroxyl groups on the adenosine ribose hydrogen bond Asp960 (sc and mc), the
260 nicotinamide ribose exhibits stabilizing hydrogen bonds only with Asn1115 (mc and sc)
261 and the nicotinamide amide contacts only Thr929 (sc) and Asp964 (sc). Thereby, together
262 with subtle but detectable changes in segments 958-966 and 981-987 contributing to the
263 DNBR, in the cofactor/ligand-monomer a shift of the cofactor towards the GluBR is
264 observed, where a novel density element becomes evident (Movie S2). It is possible to
265 locate a substrate molecule within it so that the α-carbon of the amino acid is 3.3 Å from
266 the C4 atom of the nicotinamide ring of the cofactor, thus explaining the density bridge

267 observed between them. Hence, the γ-carboxylate of the ligand establishes salt bridges
268 with Arg780 (sc).
269 Remarkably, both segment 914-924 delimiting the active site cleft and portion 886-901
270 sitting on the glutamate binding pocket adopt different conformations in the empty-,
271 cofactor- and cofactor/ligand- mL-GDH$_{180}$ monomers (Figure 2). This was in turn
272 associated with alternate conformations of the region 825-838, found better defined in the
273 electronic maps of mL-GDH$_{180}$ monomers, which allowed modeling residues 825-827 and
274 830-838 for the empty- and cofactor- monomers and residues 825 and 829-838 for the
275 cofactor/ligand-monomer. Thus, in the empty-monomer of mL-GDH$_{180}$ Arg835 points
276 toward Asp964 and Asp960, and Asp834 points toward His984. When the cofactor is
277 anchored within the DNBR and interacts with Asp964, Asp960 and His984, Arg835 and
278 Asp834 are displaced from such positions and the segment 830-838 is less tightly packed
279 against the catalytic core. When the GluBR is also occupied, the region 831-837 is packed
280 against the segment 889-894. The amino acid string 825-838 of mL-GDH$_{180}$ is found in L-
281 GDHs$_{180}$ but not in related low molecular weight enzymes (Figure 3 and Figure S4) [16].
282
283 **GluBR occupancy is linked to the coupling of the catalytic domains of two adjacent**
284 **monomers in the Closed mL-GDH$_{180}$ conformations**
285 To elucidate structural changes in the context of mL-GDH$_{180}$ tetramers, we next crossed
286 the empty-, cofactor- and cofactor/ligand-monomer classes with the tetrameric classes
287 Open, Closed1 and Closed2, thus obtaining evidence for the Open-empty-monomer,
288 Closed1-empty-monomer, Closed2-empty-monomer (3.5 Å, 3.35 Å and 3.48 Å resolution,
289 respectively), Open-cofactor-monomer, Closed1-cofactor-monomer, Closed2-cofactor-
290 monomer (3.3 Å, 3.23 Å and 3.28 Å resolution, respectively), Open-cofactor/ligand-
291 monomer, Closed1-cofactor/ligand-monomer and Closed2-cofactor/ligand-monomer (3.23
292 Å, 3.11 Å and 3.18 Å resolution, respectively) species (Figure S2). While no differences

293 were noticeable for the empty- or cofactor- monomers depending on whether they came
294 from Open, Closed1 and Closed2 mL-GDH_{180} tetramers, cryoEM maps disclosed
295 heterogeneous density within the glutamate binding pocket of cofactor/ligand-monomers.
296 The cryoEM map of the Open-cofactor/ligand-monomer accounts for the density within the
297 GluBR that is linked to that of the cofactor nicotinamide ring (Figure 4, see Figure 2 as
298 well), while the former vanishes in the area where the γ-carboxylate of the substrate
299 amino acid would be stabilized. Conversely, in the maps of the Closed1- and Closed2-
300 cofactor/ligand monomers density is found for the ligand in the GluBR mainly towards the
301 area closer to Arg780, such element being smaller for the Closed2 conformer.
302 As previously noted, changes in the active site of mL-GDH_{180} upon incubation with NAD^+
303 and L-glutamate are associated with structural changes in the segment 825-838 (Figure
304 2). Remarkably, this remodeled segment establishes an interaction with the region 704-
305 706 in the catalytic domain of a neighboring N-terminally-linked subunit, building a
306 molecular bridge in the Closed tetramers (Figure 4), with a consolidation of this in the
307 Closed2 form (Table 1). Such interaction is only observed when for one monomer there is
308 density simultaneously in both the cofactor and substrate binding pockets (Movie S3).
309 Overall, our results point out that the occupancy of the GluBR of mL-GDH_{180} is linked to
310 the coupling of the catalytic domains of two adjacent subunits, which may be the basis for
311 a regulatory mechanism of turnover.
312

313 **DISCUSSION**

314 GDHs constitute a large family of enzymes that function in all kingdoms of life at the
315 crossroad between the Krebs cycle and ammonium assimilation. While S-GDHs have
316 been studied for more than half a century, it was not until 2021 that the first experimental
317 evidence for the 3D architecture of an L-GDH was obtained [3]. In that work we determined
318 that the quaternary structure of mL-GDH_{180} is radically different from that of S-GDHs and
319 that such assembly depends on the distinctive N- and C-terminal regions found in L-GDHs
320 [3]. Here we present cryoEM evidence of up to 2.63 Å resolution for mL-GDH_{180} (Table1)
321 obtained in the presence of NAD^+ during oxidative deamination of L-glutamate.

322 We have solved the 3D structure of mL-GDH_{180} species with the DNBR and the GluBR
323 simultaneously occupied as well as NAD^+-only charged subunits (Figure 1, Figure 2 and
324 Figure 4). The binding mode of NAD^+ to mL-GDH_{180} (Figure 2 and Figure 4) is analogous
325 to that described for *Cs*GDH [15]. The adenine ring of NAD^+ is stabilized in mL-GDH_{180} by
326 hydrogen bonds with residues His984 (Pro262 in *Cs*GDH) and Tyr1079 (Asp325), the NH
327 and CO groups of the nicotinamide amide contact Asp964 (Asn240) and Thr929 (Thr209),
328 respectively, the phosphates interact with Asp964 and Val965 (Val241), while the
329 nicotinamide ribose hydrogen bonds Gly1075 (Ala321) and Asn1115 (Asn347). On the
330 other hand, the 2'-OH group of the adenosine ribose, which shares with the 3'-OH group
331 the Asp960 (Phe238) ligand and is additionally surrounded by Asp983 (Gly261) and
332 His984, is stabilized in mL-GDH_{180} in a relatively wider pocket than the equivalent in
333 *Cs*GDH [15]. Considering that His984 and Arg985 (Asp263) could potentially provide
334 stabilizing interactions for the distinctive phosphate attached to the 2'-OH in $NADP^+$, a
335 possible explanation for mL-GDH_{180} NAD^+ specificity [17,18] is that this enzyme, as well as
336 related L-GDHs [2,19–24], would have evolved the ability to positively select the cofactor
337 through the interactions established by the 2'-OH group with Asp960 and Asp983, which
338 would, in addition, exert a repulsive effect on the 2'-OP in $NADP^+$. This is consistent with

339 previous proposals that NAD^+ specificity may be dictated by interactions of the 2'-OH
340 group of the adenosine ribose with the Gly-rich loop (GxGxxA/S, as defined in L-$GDHs_{180}$
341 [2]) and with an acidic residue at the so-called position 7 (Asp983 in mL-GDH_{180}) of the
342 fingerprint region of the nucleotide binding fold [25,26].
343 In a pioneering work it was determined that amino acid specificity is determined in *Cs*GDH
344 by the interactions between the side chains of Lys89 and Ser380 with the γ-carboxylate of
345 the substrate [27]. Similarly, the position of Arg780 (Lys89) allows it to form salt bridges with
346 the γ-carboxylate of L-glutamate modeled in the GluBR of mL-GDH_{180} (Figure 2). Besides,
347 although the distance between the hydroxyl of Ser1147 (Ser380) of mL-GDH_{180} and the γ-
348 carboxylate of L-glutamate (4.3 Å) exceeds that of a hydrogen bond, the position of such
349 residue is equivalent to that of Ser360 in *Cs*GDH. Also, residues Ala886 and Val1144
350 (Ala163 and Val377), Gly814 and Ala815 (Gly122 and Gly123), Gly781 and Gly782 (Gly90
351 and Gly91) and Gly1143 (Gly376), previously highlighted for their roles in establishing
352 hydrophobic interactions with the γ- and δ-carbons of L-glutamate, shaping the L-
353 glutamate binding pocket, orienting functional groups in the catalytic center and being
354 located near the binding site of the nicotinamide ring of the dinucleotide, respectively [27],
355 are arranged in cofactor/ligand- mL-GDH_{180} monomers in a manner similar to that
356 observed for *Cs*GDH. Overall, these observations highlight the preservation of the
357 determinants involved in amino acid specificity in mL-GDH_{180} (and related L-GDHs; see
358 Figure S4 and [2]) as compared to *Cs*GDH (and related S-GDHs).
359 Given the conservation of active site residues, catalysis would proceed by the same
360 mechanism in S-GDH and L-GDH [3]. Our atomic model of the mL-GDH_{180} cofactor/ligand-
361 monomer was built in an attempt to explain the observed density within the GluBR (Figure
362 2). According to this, the α-carboxylate and amino groups of L-glutamate would adopt in
363 the GluBR of mL-GDH_{180} a somewhat different orientation to that described for *Cs*GDH [27].
364 On the one hand, even thought the α-carboxylate of L-glutamate points towards Lys806

365 (Lys113), the distance between them (4.1 Å) is relatively long. Besides, the α-carboxylate
366 of the substrate is 6.4 Å away from the side chain of Gln803 (Gln110). On the other hand,
367 the amino group of L-glutamate is 4.9 Å away from the carbonyl of Ala887 (Gly164) and
368 6.7 Å away from the side chain of the catalytic Asp888 (Asp165). It should be noted,
369 however, that although packing of the region 825-838 against the segment 889-894 would
370 stabilize the position of Asp888, the carboxylate of this residue is not completely defined in
371 the density maps of the mL-GDH_{180} cofactor/ligand-monomer. Nevertheless, experimental
372 data for the cofactor/ligand-monomer (Figure 2 and Figure 4) reveal density consistent
373 with positioning of a group, modeled as the α-carbon of L-glutamate, 3.2 Å from the C4
374 atom of the cofactor nicotinamide, and density 3-3.5 Å from the Ala887 carbonyl, where
375 the leaving NH_3 group would be found upon catalysis.
376 The accumulated cryoEM evidence for mL-GDH_{180} ([3] and this work) indicates that this
377 enzyme has a very dynamic behavior. In the absence of any ligand, two tetrameric forms
378 of mL-GDH_{180} were found [3], named Open and Closed (4.19 and 6.6 Å resolution,
379 respectively). In the present work we used a saturating (4 mM) concentration of NAD^+ and
380 a sub-saturating (42 mM) concentration of L-glutamate (see also Figure S1). Consistent
381 with expectations, evidence of DNBR loading was found in all detected tetrameric forms of
382 the enzyme (Figure 1). Thus, under the conditions tested mL-GDH_{180} samples the
383 conformational space in such a way that the stabilization of the Closed tetramers is
384 promoted. The segment 825-838 adopts alternative conformations depending on the
385 anchoring of the cofactor to the DNBR as well as the presence of L-glutamate (or
386 derivatives thereof) in the GluBR (Figure 2). The geometry of the segment 825-838 in mL-
387 GDH_{180} monomers with the GluBR and the DNBR simultaneously loaded (cofactor/ligand-
388 monomers) is compatible with the consolidation of a contact between such a region and
389 the zone 704-706 of a neighboring subunit linked by the N-terminal region (Figure 4).

390 Unlike for S-GDH [27,28], we have not found evidence of changes in the relative positions of
391 the SDI and SDII in the catalytic domain of mL-GDH$_{180}$. Instead, we have detected
392 changes in inter-monomeric couplings involving residues 650 (in the HM3) and 790 (in the
393 catalytic domain) as well as regions 825-838 and 704-706 (both in the catalytic domain) of
394 adjacent mL-GDH$_{180}$ subunits. These, in turn, are accompanied by adjustments in the
395 interfaces provided by the ACT*3 and C-terminal domains of the enzyme. Transitions of
396 the tertiary and quaternary structure at long distances from the active site must be much
397 slower than catalysis and are, therefore, detectable in our experiment. Although given the
398 nature of our data we cannot draw conclusions about positional and/or compositional
399 heterogeneity within the GluBR and the DNBR of mL-GDH$_{180}$, and therefore not about
400 singular events during the enzyme-catalyzed deamination, it is reasonable to expect
401 catalysis to occur when there is evidence of simultaneous loading of the two regions
402 (cofactor/ligand-monomer, Figure 4), with the cofactor approaching the substrate binding
403 pocket (Figure 2). Certainly, for catalysis to take place, a relatively rapid and local
404 conformational change must occur that allows the side chain of the catalytic Asp888 to
405 approach the amino group of the substrate for proton abstraction in the first stage of the
406 reaction [27]. Notably, in the absence of effectors, we have not found evidence of
407 cooperativity for mL-GDH$_{180}$-catalyzed L-glutamate oxidation, neither at optimal pH (6.5-
408 7.0) nor at other pHs, as tested in buffers of diverse chemical nature. However, it is
409 intriguing whether [3] and how [17] this might be different in the presence of modulators of mL-
410 GDH$_{180}$ activity.
411 We have discovered that ligand binding to the orthosteric site of mL-GDH$_{180}$ is linked to
412 changes in the enzyme tertiary structure that affect the arrangement of oligomeric
413 interfaces nanometers away from the active site [29]. Allosteric regulation usually involves
414 the inverse pathway, with the binding of molecules to an allosteric site modulating the
415 catalytic center. It is interesting to consider whether and how the binding of natural or

416 designed molecules to the 825-838 and/or 704-706 segments of mL-GDH_{180} could impact
417 on catalysis and how the occupancy of the enzyme active site could make such regulation
418 more or less permissive [30]. Our work opens new perspectives for atomic resolution studies
419 on catalysis and regulation of GDHs of medical and industrial relevance.
420
421

422 **REFERENCES**

423 1. Li, M., Li, C., Allen, A., Stanley, C. A. & Smith, T. J. Glutamate dehydrogenase:
424 Structure, allosteric regulation, and role in insulin homeostasis. *Neurochemical*
425 *Research* **39**, 433–445 (2014).

426 2. Miñambres, B., Olivera, E. R., Jensen, R. A. & Luengo, J. M. A new class of
427 glutamate dehydrogenases (GDH): Biochemical and genetic characterization of the
428 first member, the AMP-requiring NAD-specific GDH of Streptomyces clavuligerus. *J.*
429 *Biol. Chem.* **275**, 39529–39542 (2000).

430 3. Lázaro, M. *et al.* 3D architecture and structural flexibility revealed in the subfamily of
431 large glutamate dehydrogenases by a mycobacterial enzyme. *Commun. Biol.* **4**, 684
432 (2021).

433 4. Lang, E. J. M., Cross, P. J., Mittelstädt, G., Jameson, G. B. & Parker, E. J. Allosteric
434 ACTion: The varied ACT domains regulating enzymes of amino-acid metabolism.
435 *Curr. Opin. Struct. Biol.* **29**, 102–111 (2014).

436 5. Möglich, A., Ayers, R. A. & Moffat, K. Structure and Signaling Mechanism of Per-
437 ARNT-Sim Domains. *Structure* **17**, 1282–1294 (2009).

438 6. Gallant, J. L., Viljoen, A. J., Van Helden, P. D. & Wiid, I. J. F. Glutamate
439 dehydrogenase is required by mycobacterium bovis BCG for resistance to cellular
440 stress. *PLoS One* **11**, 1–14 (2016).

441 7. Zheng, S. Q. *et al.* MotionCor2: anisotropic correction of beam-induced motion for
442 improved cryo-electron microscopy. *Nat. Methods* **14**, 331–332 (2017).

443 8. Rohou, A. & Grigorieff, N. CTFFIND4: Fast and accurate defocus estimation from
444 electron micrographs. *J. Struct. Biol.* **192**, 216–221 (2015).

445 9. Zivanov, J. *et al.* New tools for automated high-resolution cryo-EM structure
446 determination in RELION-3. *Elife* **7**, e42166 (2018).

447 10. He, J., Li, T. & Huang, S. Y. Improvement of cryo-EM maps by simultaneous local

448 and non-local deep learning. *Nat. Commun.* **14**, 1–16 (2023).
449 11. Pettersen, E. F. *et al.* UCSF Chimera - A visualization system for exploratory
450 research and analysis. *J. Comput. Chem.* **25**, 1605–1612 (2004).
451 12. Emsley, P., Lohkamp, B., Scott, W. G. & Cowtan, K. Features and development of
452 Coot. *Acta Crystallogr. Sect. D Biol. Crystallogr.* **66**, 486–501 (2010).
453 13. Afonine, P. V. *et al.* Real-space refinement in PHENIX for cryo-EM and
454 crystallography. *Acta Crystallogr. Sect. D Struct. Biol.* **74**, 531–544 (2018).
455 14. Abramson, J. *et al.* Accurate structure prediction of biomolecular interactions with
456 AlphaFold 3. *Nature* **630**, 493–500 (2024).
457 15. Baker, P. J. *et al.* Subunit assembly and active site location in the structure of
458 glutamate dehydrogenase. *Proteins Struct. Funct. Bioinforma.* **12**, 75–86 (1992).
459 16. Britton, K. L., Baker, P. J., Rice, D. W. & Stilllman, T. J. Structural relationship
460 between the hexameric and tetrameric family of glutamate dehydrogenases. *Eur. J.*
461 *Biochem.* **209**, 851–859 (1992).
462 17. O'Hare, H. M. *et al.* Regulation of glutamate metabolism by protein kinases in
463 mycobacteria. *Mol. Microbiol.* **70**, 1408–1423 (2008).
464 18. Nott, T. J. *et al.* An intramolecular switch regulates phosphoindependent FHA
465 domain interactions in Mycobacterium tuberculosis. *Sci. Signal.* **2**, ra12 (2009).
466 19. Veronese, F. M., Nyc, J. F., Degani, Y., Brown, D. M. & Smith, E. L. Nicotinamide
467 adenine dinucleotide specific glutamate dehydrogenase of Neurospora. I.
468 Purification and molecular properties. *J. Biol. Chem.* **249**, 7922–7928 (1974).
469 20. Lu, C. D. & Abdelal, A. T. The gdhB gene of Pseudomonas aeruginosa encodes an
470 arginine-inducible NAD+-dependent glutamate dehydrogenase which is subject to
471 allosteric regulation. *J. Bacteriol.* **183**, 490–499 (2001).
472 21. Camardella, L. *et al.* The Antarctic Psychrobacter sp. TAD1 has two cold-active
473 glutamate dehydrogenases with different cofactor specificities. Characterisation of

474 the NAD+-dependent enzyme. *Comp. Biochem. Physiol. - A Mol. Integr. Physiol.*
475 **131**, 559–567 (2002).
476 22. Kawakami, R., Sakuraba, H. & Ohshima, T. Gene cloning and characterization of the
477 very large NAD-dependent L-glutamate dehydrogenase from the psychrophile
478 Janthinobacterium lividum, isolated from cold soil. *J. Bacteriol.* **189**, 5626–5633
479 (2007).
480 23. Kawakami, R., Oyama, M., Sakubara, H. & Ohshima, T. The Unique Kinetic
481 Behavior of the Very Large NAD-Dependent Glutamate Dehydrogenase from
482 Janthinobacterium lividum. *Biosci. Biotechnol. Biochem.* **74**, 884–887 (2010).
483 24. Beaufay, F. *et al.* A NAD-dependent glutamate dehydrogenase coordinates
484 metabolism with cell division in Caulobacter crescentus. *EMBO J.* **34**, 1786–1800
485 (2015).
486 25. Baker, P. J., Britton, K. L., Rice, D. W., Rob, A. & Stillman, T. J. Structural
487 consequences of sequence patterns in the fingerprint region of the nucleotide
488 binding fold. Implications for nucleotide specificity. *J. Mol. Biol.* **228**, 662–671 (1992).
489 26. Engel, P. C. Glutamate dehydrogenases: The why and how of coenzyme specificity.
490 *Neurochem. Res.* **39**, 426–432 (2014).
491 27. Stillman, T. J., Baker, P. J., Britton, K. L. & Rice, D. W. Conformational flexibility in
492 glutamate dehydrogenase: Role of water in substrate recognition and catalysis.
493 *Journal of Molecular Biology* **234**, 1131–1139 (1993).
494 28. Borgnia, M. J. *et al.* Using cryo-EM to map small ligands on dynamic metabolic
495 enzymes: Studies with glutamate dehydrogenase. *Mol. Pharmacol.* **89**, 645–651
496 (2016).
497 29. Perica, T., Chothia, C. & Teichmann, S. A. Evolution of oligomeric state through
498 geometric coupling of protein interfaces. *Proc. Natl. Acad. Sci.* **109**, 8127–8132
499 (2012).

500 30. Schulze, J. O. *et al.* Bidirectional Allosteric Communication between the ATP-
501 Binding Site and the Regulatory PIF Pocket in PDK1 Protein Kinase. *Cell Chem.*
502 *Biol.* **23**, 1193–1205 (2016).
503

ACKNOWLEDGMENTS

This work was supported by grants PICT 2019-00989 and PICT 2021-00253 from the Agencia Nacional de Promoción de la Investigación, el Desarrollo Tecnológico y la Innovación (Agencia I+D+i, Argentina) to MNL as well as grants PID2021-124074NB-I00 and PID2021-125946OB-I00 from Agencia Estatal de Investigación of Spain to MV and GJO, respectively. We also thank the Severo Ochoa Center of Excellence Accreditation CEX2021-001136-S. MNL is a career investigator from Consejo Nacional de Investigaciones Científicas y Técnicas (CONICET, Argentina). NC holds a CONICET PhD fellowship. Some of this work was performed at the Basque Resource for Electron Microscopy located at Instituto Biofisika (UPV/EHU, CSIC), supported by the Department of Science, Universities and Innovation and the Innovation Fund of the Basque Government, with additional support from MCIN (Recovery, Transformation and Resilience Plan) and the Basque Government "Biotechnology Complementary Plan Applied to Health" with funding from European Union NextGenerationEU (PRTR-C17.I1; PRTR-C17.I01.P01.S13) (AAAA_ACG_AY_2539/22_05).

AUTHOR CONTRIBUTIONS

ML produced protein, prepared EM samples, performed EM experiments, processed and analyzed EM data and performed structural analyses; NC produced protein, performed kinetic analyses, analyzed EM data and performed structural analyses; JPLA collected and analyzed EM data; RMR performed structural analyses; GJO performed structural analyses; MV designed experiments, supervised EM data collection and processing and analyzed results; MNL designed experiments, supervised biochemical experiments, refined atomic models, analyzed data and wrote the paper. All authors read and corrected the paper.

COMPETING INTERESTS

The authors declare no competing interests.

533 **FIGURES**

534 **Figure 1**

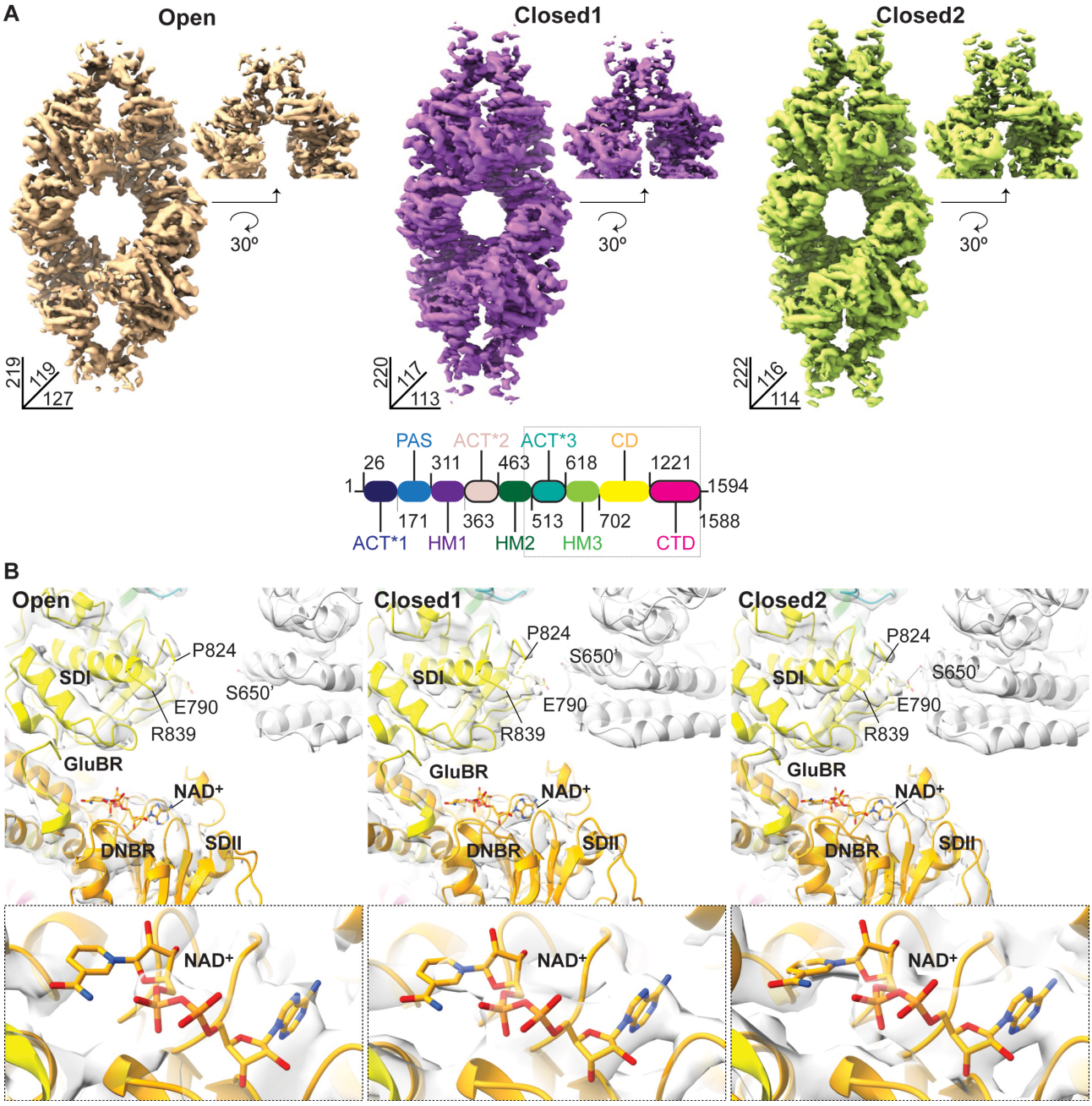

535

536 **Three conformers of mL-GDH$_{180}$ detected upon incubation with L-glutamate and**
537 **NAD$^+$ reveal modulations of the enzyme quaternary structure.** (A) CryoEM mL-GDH$_{180}$
538 maps obtained after incubating the enzyme with L-glutamate and NAD$^+$. The dimensions
539 of each conformer are provided in Å. Maps cover, for each monomer, the region indicated
540 by a dotted rectangle in the diagram shown below (residues 500-1588). ACT*, Aspartate
541 kinase-Chorismate mutase-TyrA-like; PAS, Per-Arnt-Sim; HM, helical motif; CD, catalytic

542 domain; CTD, C-terminal domain. (B) Approach of the catalytic domains of mL-GDH_{180}
543 subunits linked by the N-terminal region. Segment 825-838, poorly defined in maps of the
544 Open, Closed1 and Closed2 enzyme forms, approaches the catalytic domain in a
545 neighboring subunit. In each case, a zoomed in view of the dinucleotide binding region
546 (DNBR) is shown below. The protein is displayed in ribbon representation and cryoEM
547 maps are depicted in grey. The nicotinamide portion of the NAD^+ molecule (in sticks)
548 exhibits high mobility in all conformations. Subdomains I and II (SDI and SDII) of the
549 catalytic domain are colored in yellow and orange, respectively, whereas ACT*3 and HM3
550 motifs are shown in cyan and green, respectively, for one monomer (the one on the left),
551 with the neighboring subunit (the one on the right) shown in grey. GluBR, glutamate
552 binding region.
553

554 **Figure 2**

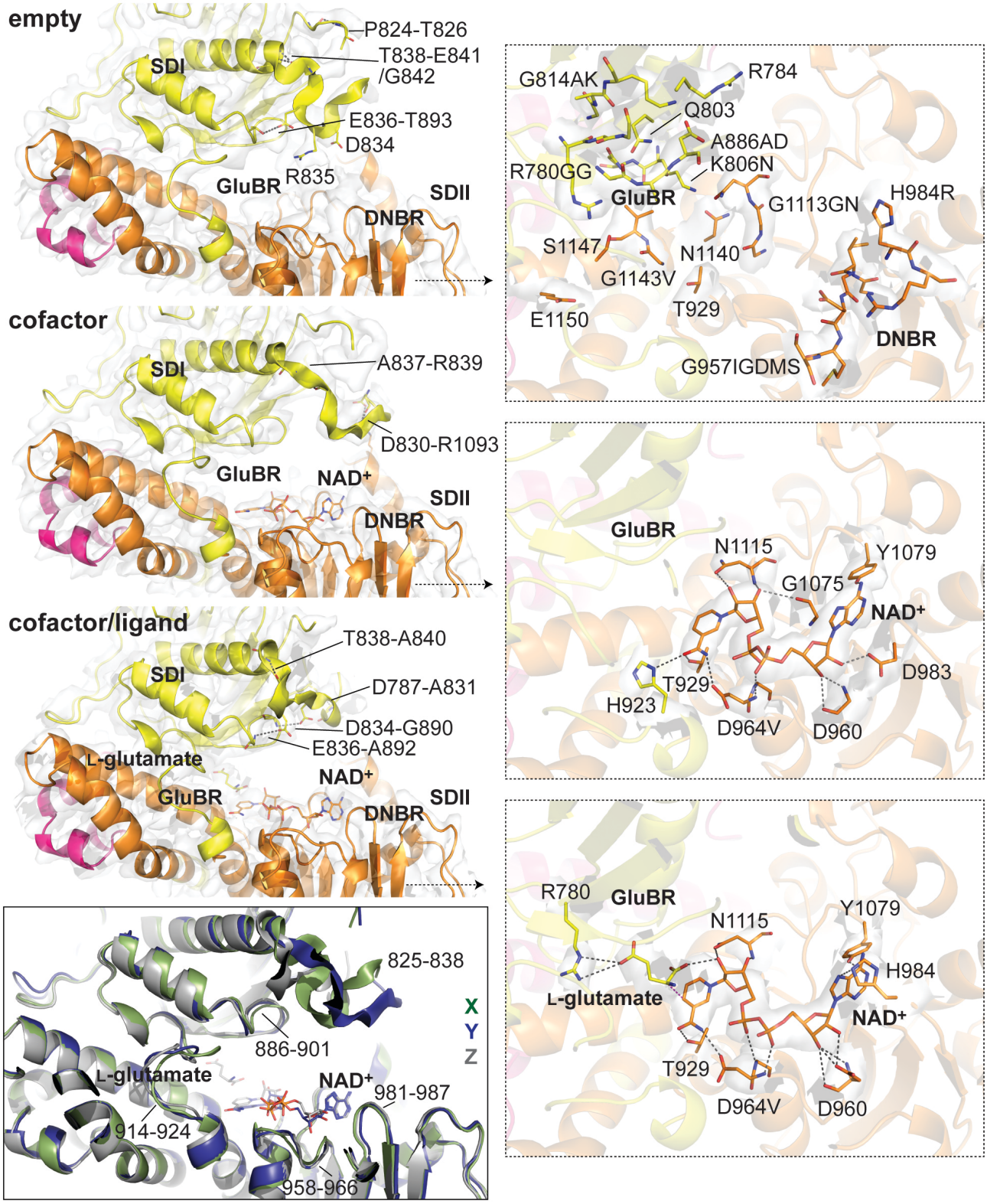

555

556 **Three conformers of mL-GDH$_{180}$ subunits reveal modulations in tertiary structure**
557 **associated with differential active site occupancies.** Alternative conformations of mL-
558 GDH$_{180}$ subunits are shown, with the active site either empty or containing NAD$^+$ or NAD$^+$
559 and L-glutamate. The average RMSD for 1122 aligned residues in pairwise comparisons

560 of the atomic models (show in ribbon representation) is 0.7 Å. NAD^+ and L-glutamate are
561 depicted as sticks as well as highlighted residues. For each species, the catalytic domain
562 subdomains I and II (SDI, residues 702-926 and 1188-1220; SDII, residues 927-1187) are
563 colored in yellow and orange, respectively. Interactions established by the segment 825-
564 838 with other portions of the polypeptide chain are shown in the panels on the left. A
565 comparison of the atomic models of the empty- (green), cofactor- (blue) and
566 cofactor/ligand-monomer (gray) is presented in the lower left corner. CryoEM maps are
567 depicted in grey. H-bonds and salt bridges are displayed as dashed lines. GluBR,
568 glutamate binding region; DNBR, dinucleotide binding region.
569

570 **Figure 3**

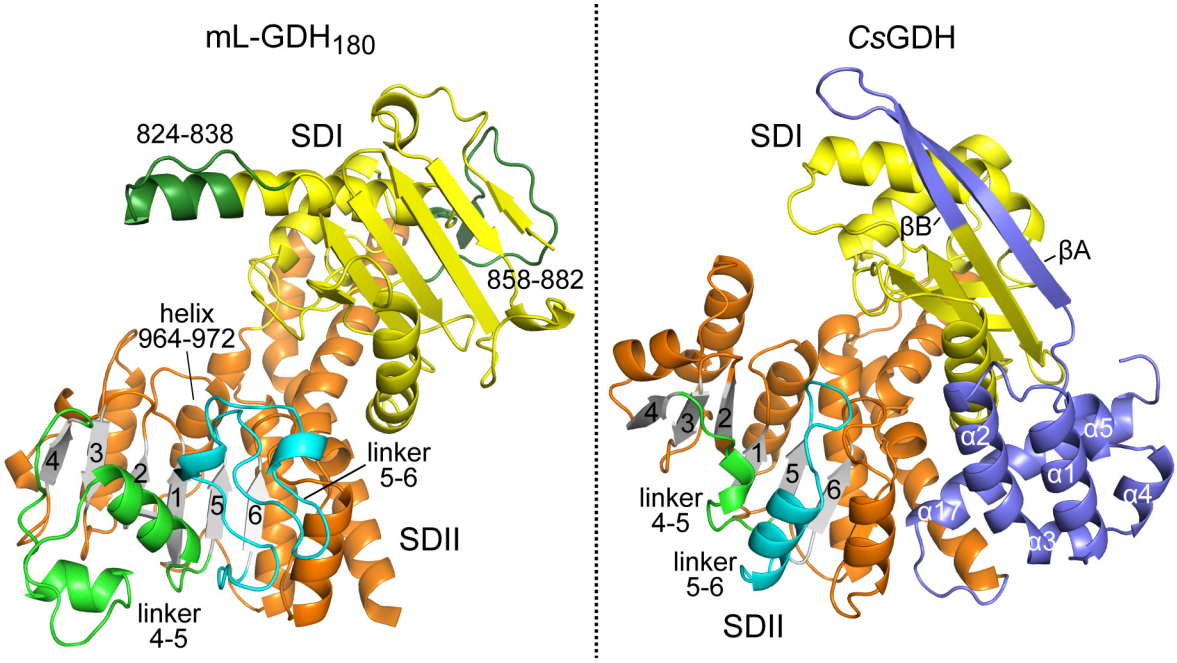

571

572 **Comparison of the catalytic domain of mL-GDH$_{180}$ with that of S-GDHs.** A monomer of
573 mL-GDH$_{180}$ is shown on the left. Segments 824-838 and 858-882 (in dark green), both
574 located in the catalytic domain subdomain I (SDI), are absent in S-GDHs [2]. For the 824-
575 838 portion coordinates were taken from a model calculated with AlphaFold 3 [14]. A
576 monomer of *Cs*GDH (*Cs*, *Clostridium symbiosum*; PDB 1BGV [27]), considered a
577 representative S-GDH, is shown on the right. The SDI of S-GDHs presents secondary
578 structure elements (in dark blue, named according to the consensus nomenclature for S-
579 GDHs) with conserved roles in oligomerization in the enzyme subfamily, which are not
580 present in mL-GDH$_{180}$ or related L-GDHs. For both mL-GDH$_{180}$ and *Cs*GDH, the six-
581 stranded 432156 β-sheet that shapes the DNBR in the catalytic domain subdomain II
582 (SDII) is shown in grey; the linker regions β4-β5 (in light green) and β5-β6 (in cyan)
583 encompass a larger number of residues in mL-GDH$_{180}$. For the two proteins, the SDI and
584 SDII are shown, except for otherwise highlighted portions, in yellow and orange,
585 respectively.

586

587 **Figure 4**

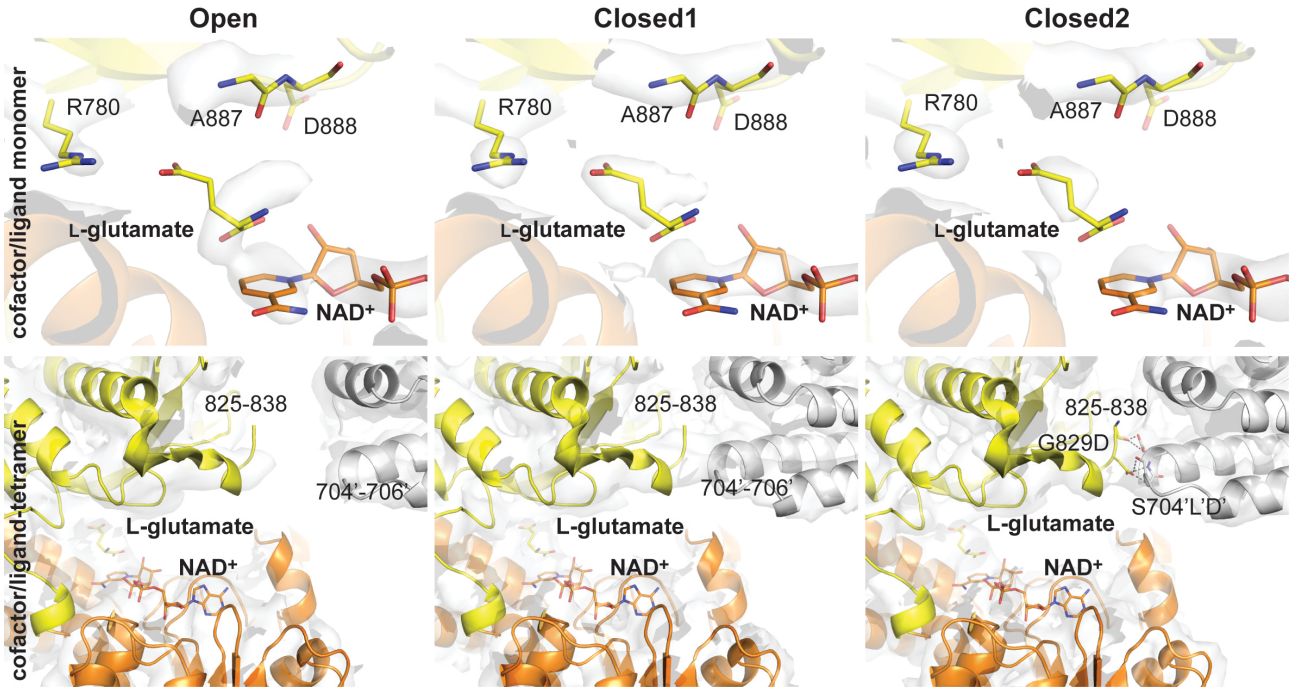

588

589 **GluBR occupancy is linked to the coupling of the catalytic domain of two adjacent**
590 **monomers in the Closed conformations.** The atomic model of the cofactor/ligand-
591 monomer of mL-GDH$_{180}$ is shown together with maps of this species obtained from Open,
592 Closed1 or Closed2 tetramers (top panel). NAD$^+$ and L-glutamate as well as highlighted
593 residues are depicted as sticks. The catalytic domain subdomains I and II (SDI and SDII)
594 are colored in yellow and orange, respectively. In the context of tetramers containing a
595 cofactor/ligand-monomer (cofactor/ligand-tetramers; bottom panel), in a progression
596 towards the Closed1 and Closed2 conformers, the stabilization of an interaction between
597 segment 825-838 of one subunit (colored, on the left) and segment 704-706 of the
598 neighboring one (in grey, on the right) is observed. The atomic coordinates of the subunit
599 on the left correspond in each case to those of a cofactor/ligand-monomer, replacing the
600 equivalent ones presented in Figure 1. H-bonds and salt bridges are displayed as dashed
601 lines. CryoEM maps are displayed in grey.

602

603 **TABLES**

604 **Table 1. CryoEM data collection and processing.** LS, local sharpening.

	Open (EMD-52419)	**Closed1** (EMD-52420)	**Closed2** (EMD-52421)
Data collection and processing			
Magnification	130,000	130,000	130,000
Voltage (kV)	300	300	300
Electron dose (e^-/Å^2)	0.979	0.979	0.979
Defocus range (μm)	1.0-1.6	1.0-1.6	1.0-1.6
Pixel size (Å)	1.29	1.29	1.29
Symmetry imposed	D2	D2	D2
Initial particles images (no.)	667,866	667,866	667,866
Final particles images (no.)	37,641	45,998	32,441
Map resolution (Å)	3.88	3.54	3.57
FSC threshold	0.143	0.143	0.143
Map sharpening B factor (Å^2)	-50	-50	-50
Refinement			
Model resolution (Å)	3.88	3.54	3.57
Model composition			
Non-hydrogen atoms	33576	33576	33576
Protein residues	4300	4300	4300
Ligands	4 NAD^+	4 NAD^+	4 NAD^+
B factors (Å^2)			
Protein	224.33	189.71	159.33
Ligands	273.06	208.84	186.14
R.m.s. deviations			
Bond lengths (Å)	0.001	0.002	0.002
Bond angles (°)	0.371	0.409	0.395
Validation			
MolProbity score	1.69	1.62	1.50
Clashscore	10.54	11.11	9.42
Poor rotamers (%)	0.11	0	0.11
Ramachandran plot			
Favored (%)	97.20	97.76	98.55
Allowed (%)	2.80	2.24	1.45
Disallowed (%)	0	0	0
CC (mask)	0.83	0.77	0.83
CC (box)	0.91	0.87	0.89
CC (peaks)	0.77	0.70	0.77
CC (volume)	0.82	0.76	0.82
Mean CC for ligands	0.85	0.82	0.80

605

	empty-monomer (EMD-52422)	**cofactor-monomer** (EMD-52423)	**cofactor/ligand-monomer** (EMD-52424)
Data collection and processing			
Magnification	130,000	130,000	130,000
Voltage (kV)	300	300	300
Electron dose (e^-/Å^2)	0.979	0.979	0.979
Defocus range (μm)	1.0-1.6	1.0-1.6	1.0-1.6
Pixel size (Å)	1.29	1.29	1.29
Symmetry imposed	C1	C1	C1
Initial particles images (no.)	464,320	464,320	464,320
Final particles images (no.)	131,216	168,668	112,701
Map resolution (Å)	3.07	2.95	3.12
FSC threshold	0.143	0.143	0.143
Map sharpening B factor	LS	LS	LS
Refinement			
Model resolution (Å)	3.07	2.95	3.12
Model composition			
Non-hydrogen atoms	8717	8761	8760
Protein residues	1124	1124	1123
Ligands	-	1 NAD^+	1 NAD^+/ 1 L-Glu
B factors (Å^2)			
Protein	64.32	62.58	72.09
Ligands	-	56.65	81.37
R.m.s. deviations			
Bond lengths (Å)	0.004	0.004	0.004
Bond angles (°)	0.691	0.721	0.693
Validation			
MolProbity score	1.37	1.27	1.37
Clashscore	5.53	5.16	5.80
Poor rotamers (%)	0.55	0.55	0.11
Ramachandran plot			
Favored (%)	97.68	98.48	97.77
Allowed (%)	2.32	1.52	2.23
Disallowed (%)	0	0	0
CC (mask)	0.87	0.88	0.87
CC (box)	0.89	0.89	0.89
CC (peaks)	0.81	0.81	0.79
CC (volume)	0.88	0.88	0.87
Mean CC for ligands	-	0.91	0.84

606

	Open-cofactor/ligand-monomer (EMD-52425)	**Closed1-cofactor/ligand-monomer** (EMD-52426)	**Closed2-cofactor/ligand-monomer** (EMD-52427)
Data collection and processing			
Magnification	130,000	130,000	130,000
Voltage (kV)	300	300	300
Electron dose (e^-/Å^2)	0.979	0.979	0.979
Defocus range (μm)	1.0-1.6	1.0-1.6	1.0-1.6
Pixel size (Å)	0.646	0.646	0.646
Symmetry imposed	C1	C1	C1
Initial particles images (no.)	112,701	112,701	112,701
Final particles images (no.)	33,330	46,380	32,991
Map resolution (Å)	3.23	3.11	3.18
FSC threshold	0.143	0.143	0.143
Map sharpening B factor	LS	LS	LS
Refinement			
Model resolution (Å)			
Model composition			
Non-hydrogen atoms			
Protein residues			
Ligands			
B factors (Å^2)			
Protein			
Ligands			
R.m.s. deviations			
Bond lengths (Å)			
Bond angles (°)			
Validation			
MolProbity score			
Clashscore			
Poor rotamers (%)			
Ramachandran plot			
Favored (%)			
Allowed (%)			
Disallowed (%)			
CC (mask)			
CC (box)			
CC (peaks)			
CC (volume)			
Mean CC for ligands			

607

	total-monomer (EMD-52428)	**Closed2-cofactor/ligand-tetramer** (EMD-52429)
Data collection and processing		
Magnification	130,000	130,000
Voltage (kV)	300	300
Electron dose (e^-/Å^2)	0.979	0.979
Defocus range (μm)	1.0-1.6	1.0-1.6
Pixel size (Å)	0.646	1.29
Symmetry imposed	C1	C1
Initial particles images (no.)	464,320	112,701
Final particles images (no.)	464,320	32,991
Map resolution (Å)	2.63	4.1
FSC threshold	0.143	0.143
Map sharpening B factor	LS	-50
Refinement		
Model resolution (Å)	2.63	
Model composition		
Non-hydrogen atoms	8683	
Protein residues	1113	
Ligands	1 NAD^+	
B factors (Å^2)		
Protein	56.19	
Ligands	48.51	
R.m.s. deviations		
Bond lengths (Å)	0.002	
Bond angles (°)	0.467	
Validation		
MolProbity score	1.39	
Clashscore	7.12	
Poor rotamers (%)	0.55	
Ramachandran plot		
Favored (%)	99.10	
Allowed (%)	0.90	
Disallowed (%)	0	
CC (mask)	0.80	
CC (box)	0.68	
CC (peaks)	0.65	
CC (volume)	0.78	
Mean CC for ligands	0.81	

608